

potential, $K_{IG} = 0.656 \text{ MPa}\sqrt{\text{m}}$. By direct atomistic simulation, we obtain $K_{IG} = 0.646 \text{ MPa}\sqrt{\text{m}}$, the agreement being a measure of our self-consistency.

Finding the MEPs and associated activation energies for bond rupture requires probing the potential energy surface of the system in a $3N$ -configurational space under an applied load K_I (boundary displacements constrained). We apply the Nudged Elastic Band method (NEB) [15] for sampling reaction pathways. Two local energy minima on the same potential energy surface mediated by K_I are identified by energy minimization; these correspond to equilibrium configurations before and after uniform crack extension in the x_1 direction by one atomic spacing (both would have the same energy at K_{IG}). A discretized elastic band consisting of a number of system replicas is then employed to connect the two states. With appropriate relaxation [15], the elastic band converges to the MEP.

For the present simulation cell with 20 bonds along the initially straight crack front, the most energetically favored pathway for the front to advance by one atomic spacing is found to involve the breaking of 20 bonds *sequentially*. Adopting this sequence as a reaction coordinate, we determine the system energy along this path. We show in Fig. 2(a) (blue upper curve) the energy change in going to the final configuration, also a straight crack front and a local energy minimum. The normalized reaction coordinate s is defined such that each integer number s labels a locally equilibrated state with s broken bonds on the crack front. Between s and $s + 1$, the coordinate denotes a normalized hyperspace arc length along the MEP for breaking the $(s + 1)$ -th bond. Each circle gives the energy, relative to the equilibrium state of a straight crack front, of a metastable crack front with s broken bonds. The barrier between two adjacent circles shows the energy variation along the MEP of breaking one more bond: $s \rightarrow s + 1$. For clarity, we use an interpolated curve to represent the calculated energies of 15 relaxed replica configurations [15] between the two adjacent circles. One sees in Fig. 2(a) the energy change is a series of barriers, each describing a particular bond rupture, and is intrinsic to the lattice structure and the nature of bonding, superposed on a smooth profile given by the envelope curve connecting the red circles. Notice that at an applied load equal to the Griffith value of K_{IG} , the initial ($s = 0$) and final ($s = 20$) configurations have the same energy by definition. If the loading is greater or less than K_{IG} , the final configurations would have energy lower or higher than the initial configuration.

Before discussing the MEP further, we show in Fig. 2(b) the profile of the crack front for a state of local energy minimum with ten broken bonds ($s = 10$). To visualize the discrete data from atomistic simulation, a continuous field of crack opening displacement across the two adjacent (111) cleavage planes is rendered by cubic-spline interpolation of the opening displacements at dis-

crete lattice sites. Two rather sharp kinks can be seen on each side of the crack front. Thus the energy variation shown in Fig. 2(a) can be interpreted in terms of the energetics of kink-pair formation and kink migration. We write the total energy change ΔE of the system (in reference to a straight crack front) for states on the envelope curve as the sum of two contributions, the elastic interaction E_{el} between two kinks of opposite signs separated by d_K and twice the self energy E_K of an individual kink. Thus, for the ideal situation of a kink pair embedded in an infinitely long, perfectly straight crack front, one has

$$\Delta E(d_K) = E_{el}(d_K) + 2E_K, \quad (1)$$

where d_K is the double-kink separation. In Eq. (1), $E_{el}(d_K)$ will asymptotically vanish as d_K increases. E_K , containing all the remaining atomistic energetic information, can be interpreted as the formation energy of an

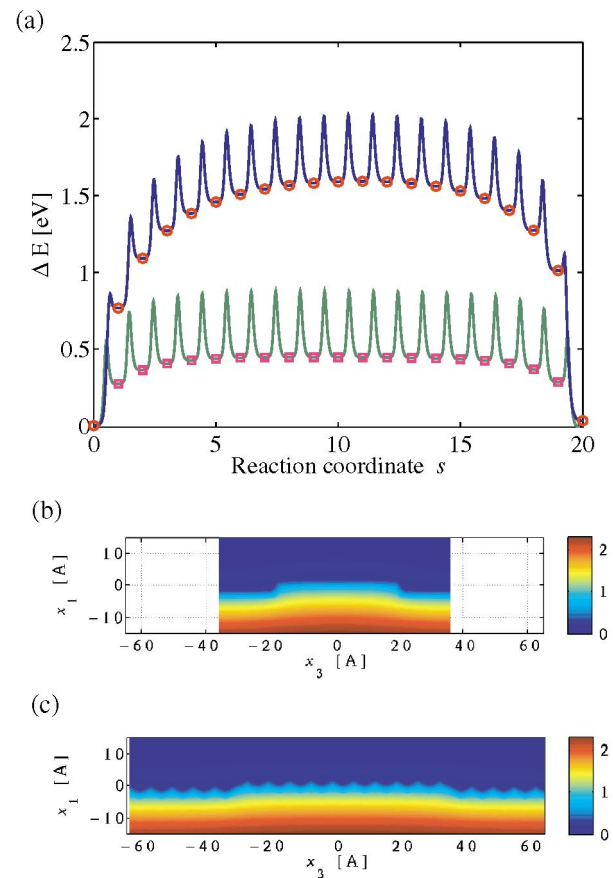


FIG. 2 (color). Energetics and geometry of crack-front bond ruptures. (a) The MEPs for the (111)[$\bar{1}\bar{1}0$] crack (blue upper curve) and the (111)[112] crack (green lower curve) at the respective Griffith loads; (b) distribution of the opening displacement across the (111) cleavage plane for the (111)[$\bar{1}\bar{1}0$] crack with ten broken bonds, normalized by the interplanar spacing $d_0 = 2.35 \text{ \AA}$; (c) same as (b), except for the (111)[112] crack.

isolated kink. Remember that “bond-to-bond roughness”, as shown in Fig. 2(a), needs to be superimposed onto Eq. (1) to represent the entire energy path.

From the upper curve in Fig. 2(a), the self energy E_K is estimated from the plateau portion of the envelope curve to be about 0.80 eV. This value is very close to an estimate of 0.81 eV using a larger simulation cell consisting of 30 unit cells along the crack front. Figure 2(a) shows that increasing d_K beyond $l/2$ will cause ΔE to decrease. This is due to the attractive image interactions associated with the use of periodic boundary condition. Fortunately, the numerical results show that $E_{el}(d_K)$ is a rapidly decreasing function with d_K , so even in the presence of image interactions we can extract E_K to be around 0.8 eV at K_{IG} .

In our interpretation of the double-kink mechanism of crack-front advancement, the energy barriers to bond rupture become barriers to kink migration. Our calculation shows that the barriers decrease, from 0.86 eV for breaking the first bond to 0.44 eV for breaking the tenth bond. As the number of broken bonds, i.e., d_K , increases, the migration barrier approaches an asymptotic value corresponding to the activation energy for the migration of an isolated kink, denoted by W_K , which can be estimated from the barrier for breaking the tenth bond, 0.44 eV. This is a rather substantial secondary energy barrier. As a result, motion of the crack tip can be expected to be sluggish.

As the applied load K_I increases beyond K_{IG} , the potential energy landscape of the system will be biased toward a forward transition. At the *athermal* critical load, denoted by K_I^m , the activation energy for breaking the first bond at the straight crack front vanishes. Examination of the computed MEPs at different loads indicates that the barrier for breaking the first bond decreases the slowest among all the barriers. Hence, beyond the critical load K_I^m , kink-pair nucleation as well as subsequent kink migrations leading to cleavage fracture will occur spontaneously without the aid of thermal fluctuations.

To determine K_I^m , we increase the loading incrementally above K_{IG} . When the load reaches $K_I \approx 0.90 \text{ MPa}\sqrt{\text{m}}$, we find it no longer possible to obtain a relaxed initial state geometrically similar to the configurations at lower loads; the system tends to relax to another local energy minimum corresponding to a different deformation mode, amorphization by formation of new crack-tip ring structures. Since our interest is to study the transition pathway for cleavage fracture on the (111) plane, we leave the issue of competition among different deformation modes to a future investigation. Nonetheless, we can estimate K_I^m by extrapolating from the barrier heights obtained at lower loads, as shown in Fig. 3. The value of K_I^m obtained in this manner is about $1.0 \text{ MPa}\sqrt{\text{m}}$. In terms of the ratio K_I^m/K_{IG} , we can define a lattice trapping range, an effect intrinsic to the discrete nature

of a crystal lattice [7]. Our value of 1.55 is of course specific to the interatomic interaction model used in this work.

Although the $\{111\}\langle 1\bar{1}0\rangle$ crack propagating in the $\langle 11\bar{2}\rangle$ direction is the most frequently studied, fractography observations of the cleavage surface indicate that a $\{111\}$ cleavage crack prefers to propagate in the $\langle 110\rangle$ direction [24]. The preference of propagation direction, called *propagation anisotropy*, has been explained by comparing orientation-dependent lattice trapping ranges of 2D crack configurations [12,13]. Here, we point to a different manifestation of this effect in the energies of kink-pair formation and migration on a crack front.

Consider the (111)[$11\bar{2}$] crack extending along the [$1\bar{1}0$] direction. The Griffith load K_{IG} for this orientation, determined from direct atomistic calculation, is $0.643 \text{ MPa}\sqrt{\text{m}}$, compared to a theoretical value of $0.654 \text{ MPa}\sqrt{\text{m}}$. The lower curve in Fig. 2(a) shows the MEP of sequentially breaking 20 bonds along the (111)[$11\bar{2}$] crack front. Comparing to the earlier result for the (111)[$1\bar{1}0$] crack, we find significantly different kink-pair formation energy at about 0.22 eV versus 0.8 eV, while the migration energies are similar.

As the applied load increases by about the same ratio beyond K_{IG} , the activation energy required to extend the (111)[$11\bar{2}$] crack is consistently lower than that for the (111)[$1\bar{1}0$] crack. To estimate the lattice trapping range for the former, we again obtain the athermal load by extrapolation. As shown in Fig. 3, a value of $K_I^m = 0.88 \text{ MPa}\sqrt{\text{m}}$ is obtained, which then leads to $K_I^m/K_{IG} = 1.37$, a nar-

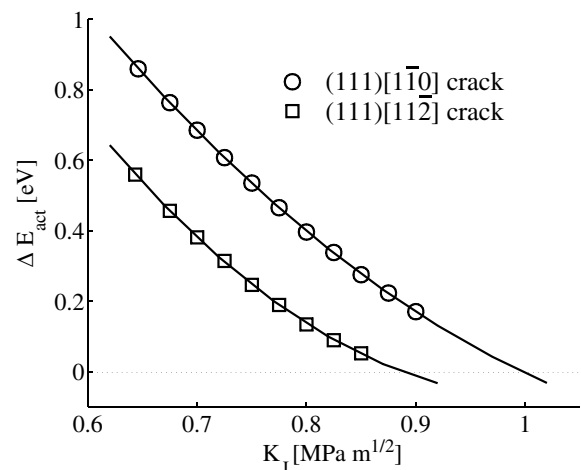


FIG. 3. Activation energy barrier ΔE_{act} as a function of load K_I for breaking the first bond at a straight crack front for two crack orientations: symbols represent the calculated data points and solid lines are the polynomial extrapolations. The athermal loads of instantaneous fracture, which can be determined from the intersections between the solid lines and dashed line, are $K_I^m = 1.0 \text{ MPa}\sqrt{\text{m}}$ for the (111)[$1\bar{1}0$] crack and $K_I^m = 0.88 \text{ MPa}\sqrt{\text{m}}$ for the (111)[$11\bar{2}$] crack, respectively.

rower lattice trapping range for the second crack orientation.

It is instructive to correlate the difference in lattice trapping range with details of the atomic configurations of the crack front. As shown in Fig. 2(c) for the (111)[11 $\bar{2}$] crack, both the leading and trailing edges of the crack front have a zigzag profile, which indicates that the second array of bonds adjacent to the crack front also have relatively large opening displacements. This configurational feature is not present in the smooth profile of the (111)[1 $\bar{1}$ 0] crack. The difference in crack-front displacements can be attributed to the bond densities along different directions on the (111) plane. Assuming the linear elastic solution is approximately correct, the bond opening displacement (in the x_2 direction) should vary sensitively with the distance (in the x_1 direction) from the crack front. The close-packed arrangement of atoms along the x_1 direction for the (111)[11 $\bar{2}$] crack means a smaller distance for the second array of bonds, and consequently larger equilibrium opening displacements and a more zigzag profile. Moreover, we believe this is consistent with the crack having a smaller kink formation energy in that one can expect the energy cost of barrier crossing by the crack-front kink to become smaller if tensile opening displacements before and after the crossing are closer.

We have presented above a reaction pathway analysis showing that a cleavage crack in Si advances via the kink mechanism, a result which we believe applies to any lattice with significant secondary Peierls barrier. That kinks should play a central role in crack-front mobility is understandable considering the structural similarity between the crack front, as the core of a crack tip, and the core of a dislocation line, along with the fact it is widely recognized that in Si, dislocations move by the nucleation and migration of kink pairs [16–18]. A previous study, using simplified models, has emphasized the role of kinks in chemically assisted fracture [2]. Exploiting the analogy between the crack front and dislocation core in an explicit and operational fashion, as suggested by our results, should be useful for future studies of deformation physics of both types of defects.

We conclude by commenting that in contrast to the present results, crack-tip evolution in the ductile mode is quite different. We have recently shown that in Cu, a reaction pathway analysis gives a detailed scenario of the emission of a dislocation loop from the crack front [19]. It is reassuring that this fundamental aspect of fracture behavior should be governed by both local atomic struc-

ture and interatomic bonding, effects that the present atomistic investigation is capable of probing.

We thank A. S. Argon for stimulating discussions. T. Z. and S. Y. acknowledge support by NSF, Honda R&D, DARPA-ONR, and the Lawrence Livermore National Laboratory. J. L. acknowledges support by Honda R&D Co., Ltd. and the OSU Transportation Research Endowment Program.

*Electronic address: syip@mit.edu

- [1] B. R. Lawn, *J. Mater. Sci.* **10**, 469 (1975).
- [2] R. Thomson, V. K. Tewary, and K. Masuda-Jindo, *J. Mater. Res.* **5**, 619 (1987); **5**, 631 (1987).
- [3] M. Marder, *J. Stat. Phys.* **93**, 511 (1998).
- [4] B. R. Lawn, *Fracture of Brittle Solids* (Cambridge University Press, Cambridge, England, 1993), 2nd ed.
- [5] S. M. Wiederhorn, *J. Am. Ceram. Soc.* **50**, 407 (1967).
- [6] J. B. Wachtman, *J. Am. Ceram. Soc.* **57**, 509 (1974).
- [7] R. Thomson, C. Hsieh, and V. Rana, *J. Appl. Phys.* **42**, 3145 (1971).
- [8] J. E. Sinclair and B. R. Lawn, *Proc. R. Soc. London A* **329**, 83 (1972).
- [9] J. E. Sinclair, *Philos. Mag.* **31**, 647 (1975).
- [10] W. A. Curtin, *J. Mater. Res.* **5**, 1549 (1990).
- [11] J. C. H. Spence, Y. M. Huang, and O. Sankey, *Acta Metall. Mater.* **41**, 2815 (1993).
- [12] R. Pérez and P. Gumbsch, *Phys. Rev. Lett.* **84**, 5347 (2000).
- [13] R. Pérez and P. Gumbsch, *Acta Mater.* **48**, 4517 (2000).
- [14] N. Bernstein and D. W. Hess, *Phys. Rev. Lett.* **91**, 025501 (2003).
- [15] H. Jónsson, G. Mills, and K. W. Jacobsen, in *Classical and Quantum Dynamics in Condensed Phase Simulations*, edited by B. J. Berne, G. Ciccotti, and D. F. Coker (World Scientific, Singapore, 1998), p. 385.
- [16] J. P. Hirth and J. Lothe, *Theory of Dislocations* (Wiley, New York, 1982).
- [17] V. V. Bulatov, S. Yip, and A. S. Argon, *Philos. Mag. A* **72**, 453 (1995).
- [18] W. Cai, V. V. Bulatov, J. F. Justo, A. S. Argon, and S. Yip, *Phys. Rev. Lett.* **84**, 3346 (2000).
- [19] T. Zhu, J. Li, and S. Yip, *Phys. Rev. Lett.* **93**, 025503 (2004).
- [20] A. N. Stroh, *Philos. Mag.* **7**, 625 (1958).
- [21] Z. Suo, *Proc. R. Soc. London A* **427**, 331 (1990).
- [22] F. H. Stillinger and T. A. Weber, *Phys. Rev. B* **31**, 5262 (1985).
- [23] M. Z. Bazant, E. Kaxiras, and J. F. Justo, *Phys. Rev. B* **56**, 8542 (1997).
- [24] A. George and G. Michot, *Mater. Sci. Eng. A* **164**, 118 (1993).